SUPPLEMENTARY MATERIAL

Introduction

No added material.

Data and Simulated Samples

No added material.

Event selection

The $\mathcal{S}$ distribution is shown for the analysis and EW-control samples in Fig. 9.

The effectiveness of the use of the variable $\mathcal{D} = (\Delta\phi(\not{p}_T, \text{jet}_1) + \Delta\phi(\not{p}_T, \text{jet}_2))/2$ can be seen in Fig. 10, where the distribution of $\mathcal{D}$ is shown for the EW control sample, dominated by events with real $\not{E}_T$, and for the MJ-enriched sample, dominated by events with $\not{E}_T$ arising from instrumental effects. For signal events, as well as for the non-MJ backgrounds, it is expected that $\mathcal{D} > \pi/2$ in the vast majority of events, whereas the MJ background events tend to be symmetrically distributed around $\pi/2$. In the analysis sample, $\mathcal{D} > \pi/2$ is therefore required.

The distributions for the pre b-tag sample dijet ΔR and $\not{H}_T/H_T$ (defined in Table III), and for the dijet invariant mass for medium b-tag and tight b-tag samples are shown in Fig. 11 for the EW-control sample and in Fig. 12 for the MJ-enriched sample.

Analysis using decision trees

The full list of the seventeen input variables to the MJ DT is given in Table III.

The MJ DT output is shown for the analysis and EW control samples after the medium b tagging requirement in Fig. 13.

The distributions for the dijet invariant mass, missing E_T, dijet ΔR and the b-tagging discriminating variable (L_{bb}) are shown in Fig. 14 for the analysis sample after the multijet veto and before any b-tagging requirement.

The full list of variables used in the SM DT is shown in Table III.

Systematic uncertainties

Systematic uncertainties are summarized in Table IV. The numbers quoted are uncertainties on total yields. The background cross sections entry represents the global effect of cross section uncertainties on the sum of backgrounds. There is no luminosity uncertainty associated with the multijet normalization since it comes from real data. The multijet is a non-negligible background component in medium b-tag sample.

In addition to the impact of these uncertainties on the integrated signal and background yields, modifications of the shapes of the final discriminants are also considered, when relevant. These originate mainly from jet corrections (energy scale, resolution and b-tagging) and also have small contributions from Monte Carlo reweightings and from parton distribution function variations.

Limit setting procedure

Figure 15 shows for $m_H = 125$ GeV the SM DT distributions after profiling. In this case, the background prediction and its uncertainties have been determined from the fit to data under the background-only hypothesis.

Higgs Search Results

No added material.

Diboson Search Results

The medium and tight b-tag SM DTs are shown in Fig. 16.

Figure 17 shows the SM DT distributions. The background prediction and its uncertainties have been determined from a fit to the data under the signal+background hypothesis.

Figure 18 shows the dijet invariant mass distributions, along with the background-subtracted data. The background prediction and its uncertainties have been determined from a fit to the data under the signal+background hypothesis.

Summary

No added material.

TABLE III: Variables used as input to the decision trees, where the angles θ and ϕ are the polar and azimuthal angles defined with respect to the proton beam direction. jet_1 refers to the leading taggable jet, jet_2 refers to the next-to-leading taggable jet, j_{all} refers to any jet in the event with $p_T > 15$ GeV, pseudorapidity $|\eta| < 3.2$ and without the taggability requirement. The thrust axis is the direction obtained from the difference of the transverse momenta of the leading and next-to-leading jets. The recoil is defined in the plane transverse to the beam using i) either the amount of missing transverse energy that remains after removal of the two leading jets, ii) or the sum of all good jet transerse momenta in the half plane opposite to the one containing the dijet system (with respect to the thrust axis). Among these two possible recoil definitions, the one that has the larger component along the direction orthogonal to the thrust is chosen.

Variables used in the MJ DT
$\Delta\phi(\text{jet}_1, \text{jet}_2)$
η of jet_1
$\not\!\!E_T$
$\not\!\!E_T$ significance
$\min \Delta\phi(\not\!\!E_T, j_{\text{all}})$
$\max \Delta\phi(\not\!\!E_T, j_{\text{all}}) + \min \Delta\phi(\not\!\!E_T, j_{\text{all}})$
$\max \Delta\phi(\not\!\!E_T, j_{\text{all}}) - \min \Delta\phi(\not\!\!E_T, j_{\text{all}})$
$\not\!\!H_T$(vectorial sum of j_{all} p_T)
$\not\!\!H_T / H_T$ (with H_T the scalar sum of j_{all} p_T)
Asymmetry between $\not\!\!E_T$ and $\not\!\!H_T$: $(\not\!\!E_T - \not\!\!H_T)/(\not\!\!E_T + \not\!\!H_T)$
$\not\!\!E_T$ component along the thrust axis
$\not\!\!E_T$ component perpendicular to the thrust axis
Sum of the signed components of the dijet and recoil momenta along the thrust axis
Sum of the signed components of the dijet and recoil momenta perpendicular to the thrust axis
Centrality (ratio of the scalar sum of jet_1 and jet_2 p_T to the sum of their energies)
θ angle of the dijet system
Polar angle of jet_1 boosted to the dijet rest frame with respect to the dijet direction in the laboratory
Variables used in the SM DT
Dijet mass
Dijet transverse mass
jet_1 p_T
jet_2 p_T
Scalar sum of jet_1 and jet_2 p_T
η of jet_1
η of jet_2
$\Delta\eta(\text{jet}_1, \text{jet}_2)$
$\Delta\phi(\text{jet}_1, \text{jet}_2)$
$\Delta R(\text{jet}_1, \text{jet}_2)$
p_T weighted $\Delta R(\text{jet}_1, j_{\text{all}})$
p_T weighted $\Delta R(\text{jet}_2, j_{\text{all}})$
H_T(scalar sum of j_{all} p_T)
$\not\!\!H_T$(vectorial sum of j_{all} p_T)
$\not\!\!H_T / H_T$
$\Delta\phi(\not\!\!E_T, \text{dijet})$
θ angle of jet_1 boosted to the dijet rest frame
Polar angle of jet_1 boosted to the dijet rest frame with respect to the dijet direction in the laboratory
$\min \Delta\phi(\not\!\!E_T, j_{\text{all}})$
$\max \Delta\phi(\not\!\!E_T, j_{\text{all}}) + \min \Delta\phi(\not\!\!E_T, j_{\text{all}})$
Dijet p_T
$\Delta\phi(\not\!\!E_T, \text{jet}_1)$

TABLE IV: Systematic uncertainties, in percent, of the overall signal and background yields. "Jet EC" and "Jet ER" stand for jet energy calibration and resolution respectively. "Jet R&T" stands for jet reconstruction and taggability. "Signal" includes ZH and WH production and is shown for $m_H = 125$ GeV.

Systematic Uncertainty	Signal (%)	Background (%)
Medium b-tag		
Jet EC - Jet ER	± 0.9	± 1.9
Jet R&T	± 2.9	± 2.9
b Tagging	± 0.6	± 3.7
Trigger	± 2.0	± 1.9
Lepton Identification	± 0.8	± 0.9
Heavy Flavor Fractions	–	± 8.5
Cross Sections	± 7.0	± 9.8
Luminosity	± 6.1	± 5.8
Multijet Normalilzation	–	± 1.2
Total	± 10.0	± 14.2
Tight b-tag		
Jet EC - Jet ER	± 1.0	± 1.8
Jet R&T	± 2.7	± 3.1
b Tagging	± 8.6	± 7.4
Trigger	± 2.0	± 2.0
Lepton Identification	± 0.9	± 1.1
Heavy Flavor Fractions	–	± 11.1
Cross Sections	± 7.0	± 10.0
Luminosity	± 6.1	± 6.1
Multijet Normalilzation	–	± 0.1
Total	± 13.2	± 16.9

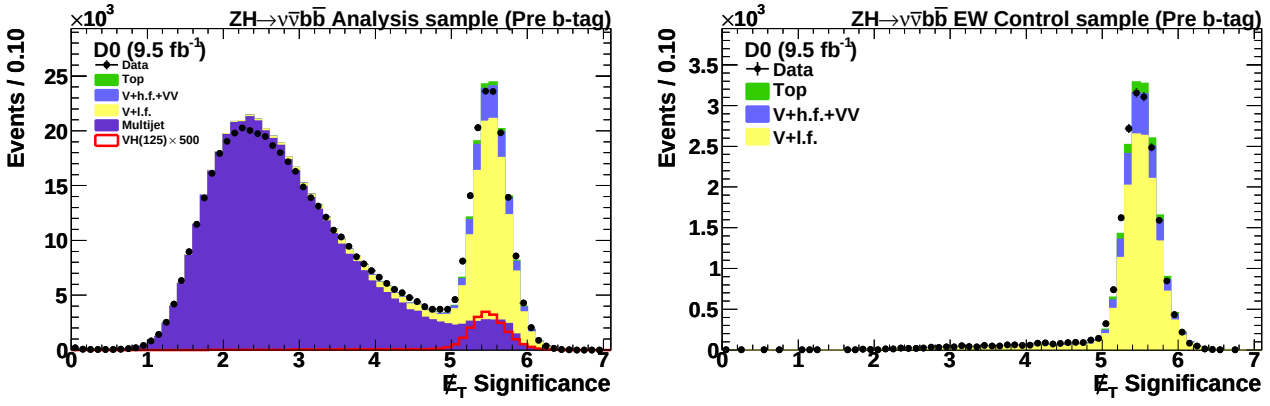

(a) (b)

FIG. 9: Missing E_T significance in (a) the analysis and (b) the EW-control samples without the requirement that the significance be larger than 5. The data are shown as points and the background contributions as histograms: dibosons are labeled as "VV," "V+l.f." includes $(W/Z)+(u,d,s,g)$ jets, "V+h.f." includes $(W/Z)+(b,c)$ jets and "Top" includes pair and single top quark production. In (a), the distribution for signal (VH) is multiplied by a factor of 500 and includes ZH and WH production for $m_H = 125$ GeV.

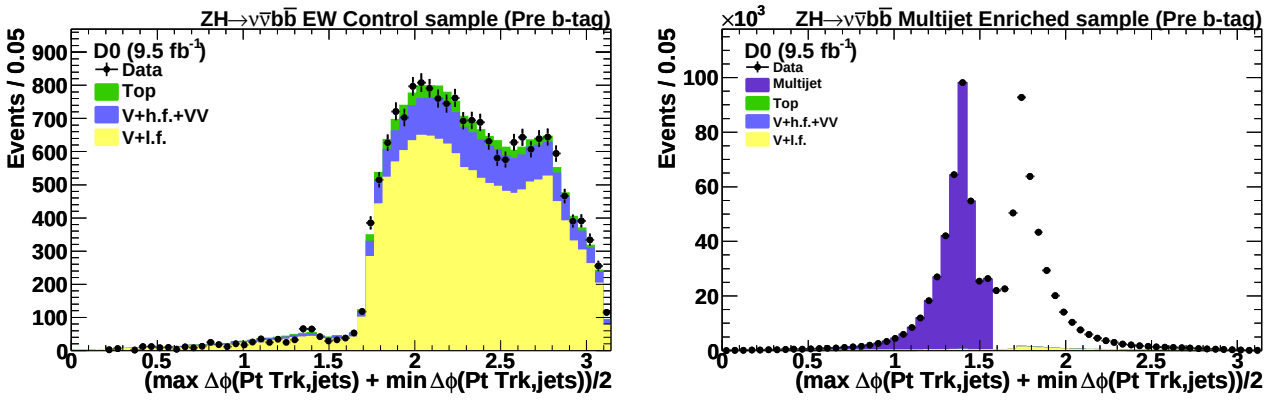

(a) (b)

FIG. 10: Distribution of $\mathcal{D}$ in (a) the EW-control sample and (b) the MJ-enriched sample, without the requirement that it be larger than $\pi/2$. The data are shown as points and the background contributions as histograms: dibosons are labeled as "VV," "V+l.f." includes $(W/Z)+(u,d,s,g)$ jets, "V+h.f." includes $(W/Z)+(b,c)$ jets and "Top" includes pair and single top quark production. In (b), the shaded region ($\mathcal{D} < \pi/2$) is used to model the events in the unshaded region ($\mathcal{D} > \pi/2$); the dip observed in the region around $\pi/2$ is due to the acoplanarity cut between the Higgs candidate jets. These distributions are shown before b tagging.

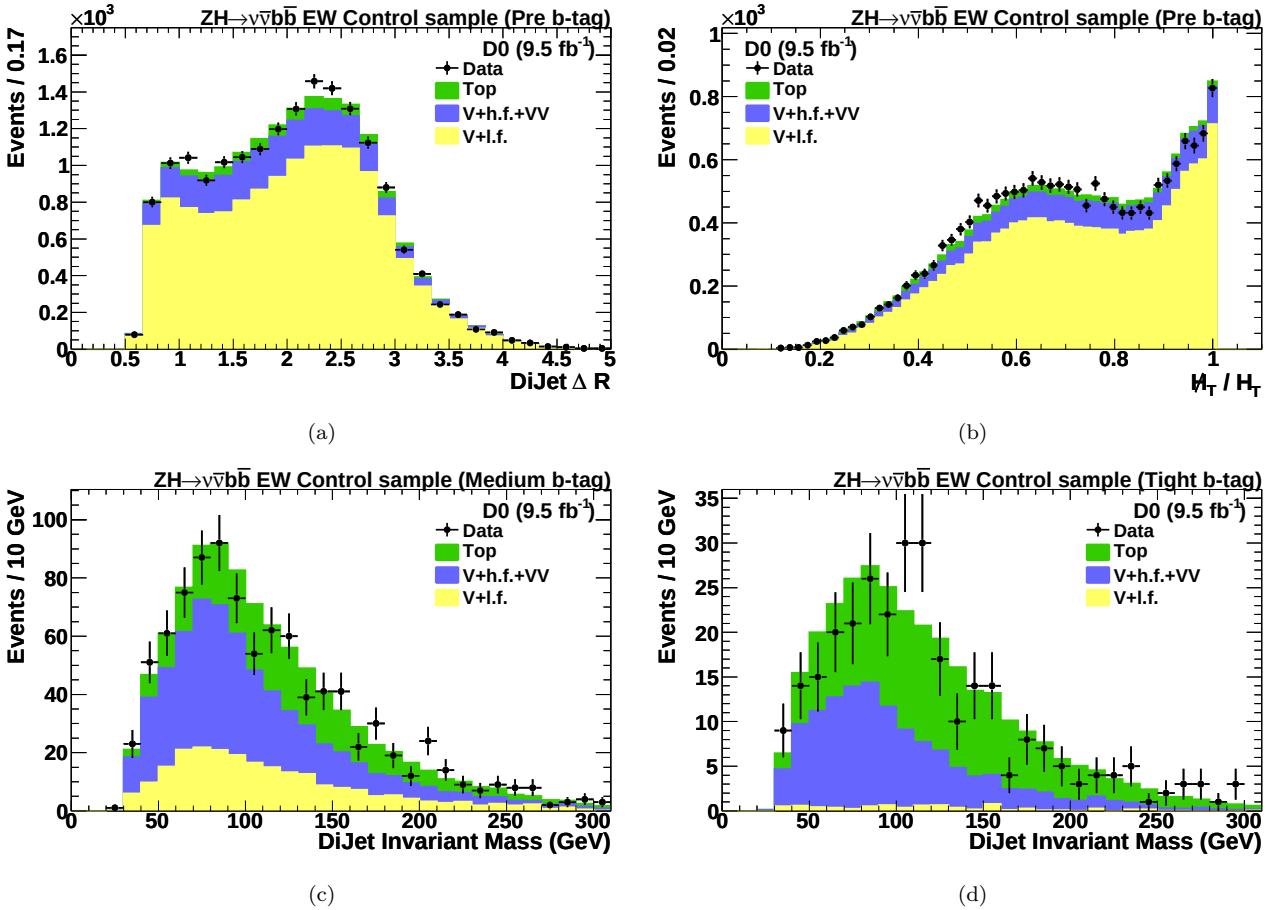

(a) (b)

(c) (d)

FIG. 11: Representative variable distributions in the EW-control sample: (a) dijet ΔR in the pre b-tag sample, (b) $\not{H}_T/H_T$ (defined in Table I) in the pre b-tag sample, (c) dijet invariant mass in the medium b-tag sample, (d) dijet invariant mass in the tight b-tag sample. The data are shown as points and the background contributions as histograms: dibosons are labeled as "VV," "V+l.f." includes $(W/Z)+(u,d,s,g)$ jets, "V+h.f." includes $(W/Z)+(b,c)$ jets and "Top" includes pair and single top quark production.

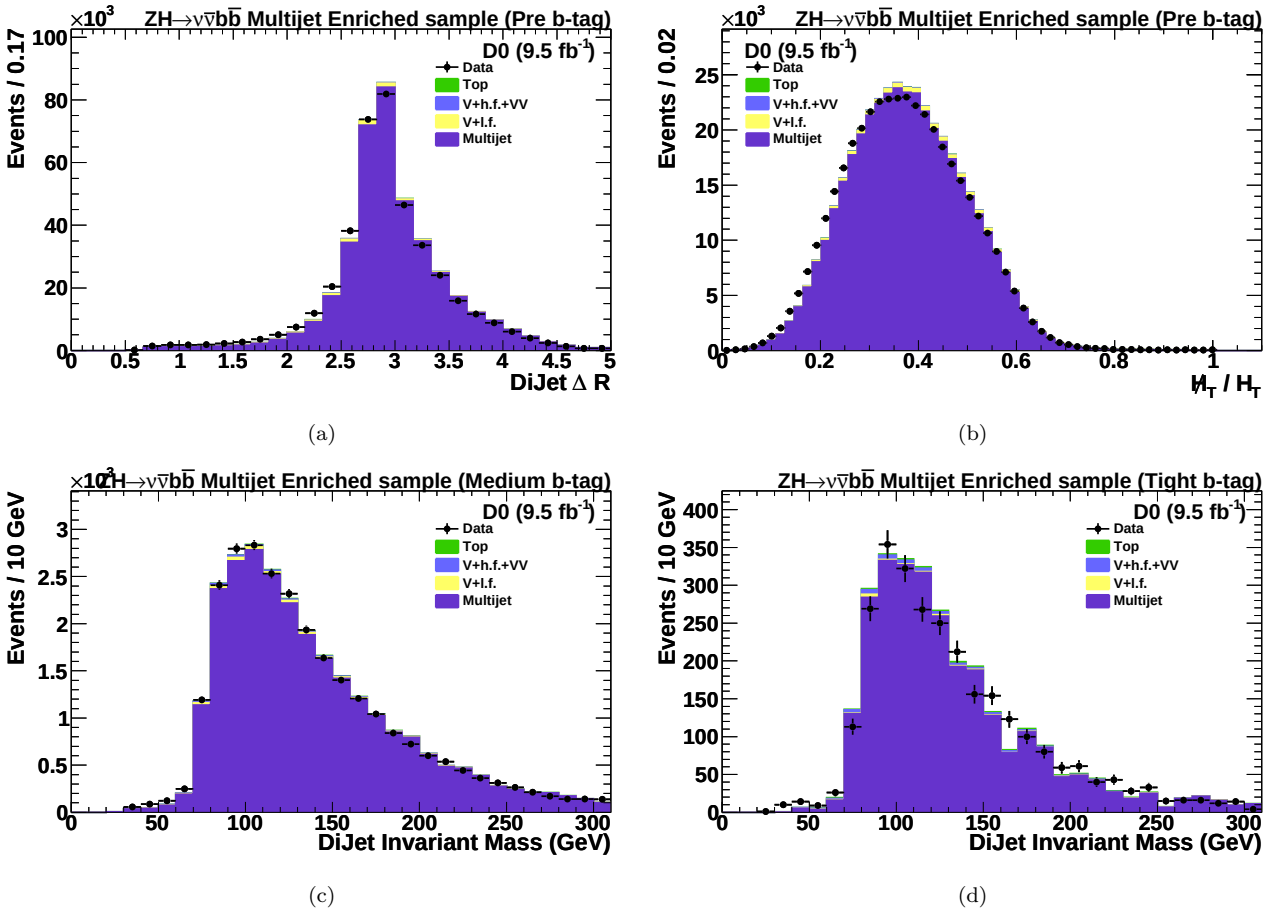

FIG. 12: Representative variable distributions in the MJ-enriched sample: (a) dijet ΔR in the pre b-tag sample, (b) $\not{H}_T/H_T$ (defined in Table I) in the pre b-tag sample, (c) dijet invariant mass in the medium b-tag sample, (d) dijet invariant mass in the tight b-tag sample. The data with $\mathcal{D} > \pi/2$ are shown as points and the background contributions as histograms: dibosons are labeled as "VV," "V+l.f." includes $(W/Z)+(u,d,s,g)$ jets, "V+h.f." includes $(W/Z)+(b,c)$ jets and "Top" includes pair and single top quark production. The "multijet" histogram is obtained from the data with $\mathcal{D} < \pi/2$

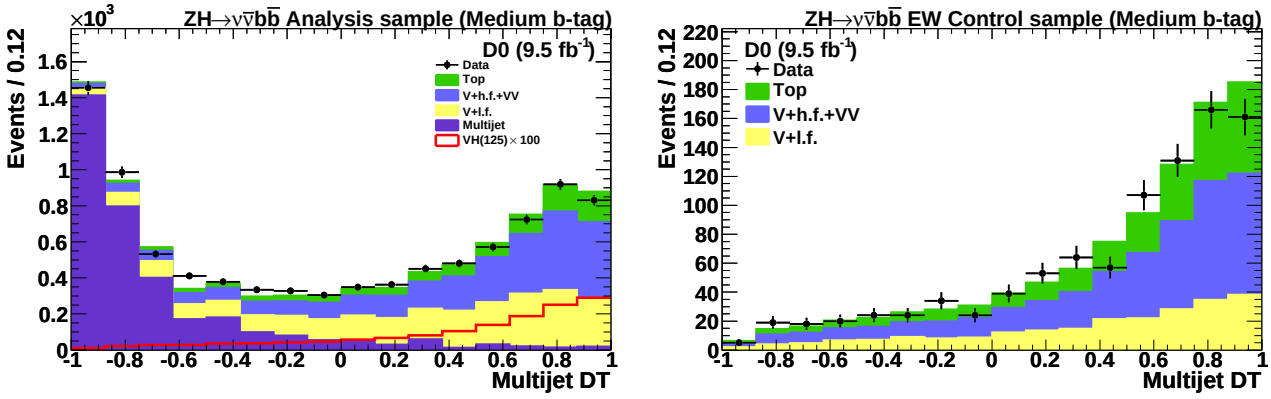

FIG. 13: MJ DT output after the medium b-tagging requirement in the (a) analysis sample and (b) EW-control sample. The distribution for signal (VH), shown for $m_H = 125$ GeV, is multiplied by a factor of 100 and includes ZH and WH production. The data are shown as points and the background contributions as histograms: dibosons are labeled as "VV," "V+l.f." includes $(W/Z)+(u,d,s,g)$ jets, "V+h.f." includes $(W/Z)+(b,c)$ jets and "Top" includes pair and single top quark production.

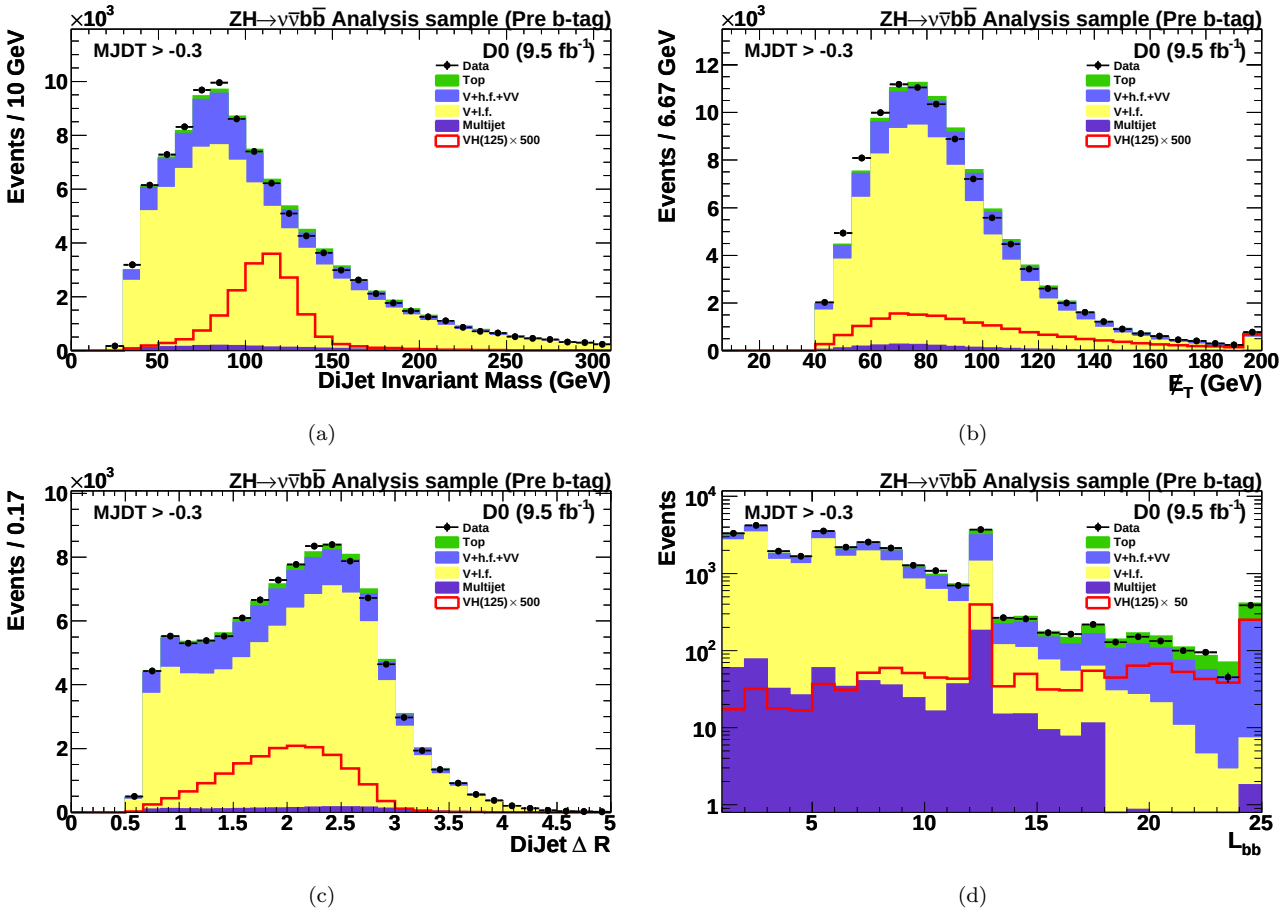

FIG. 14: Representative variable distributions in the analysis sample after the multijet veto and before any b tagging requirement: (a) dijet invariant mass, (b) missing E_T, (c) dijet ΔR, (d) b-tagging discriminating variable (L_{bb}). The bin at zero is surpressed in this plot due to the large number of entries, mostly from pairs of light jets. The relatively high number of events observed at $L_{bb} = 12$ comes mainly from events with one untagged jet and one very tightly b-tagged jet; the bin at $L_{bb} = 24$ comes from events with two very tightly b-tagged jets. The distributions for signal (VH), which are multiplied by a factor of 500 for (a)–(c) and 50 for (d), include ZH and WH production for $m_H = 125$ GeV. The data are shown as points and the background contributions as histograms: dibosons are labeled as "VV," "V+l.f." includes $(W/Z)+(u, d, s, g)$ jets, "V+h.f." includes $(W/Z)+(b, c)$ jets and "Top" includes pair and single top quark production.

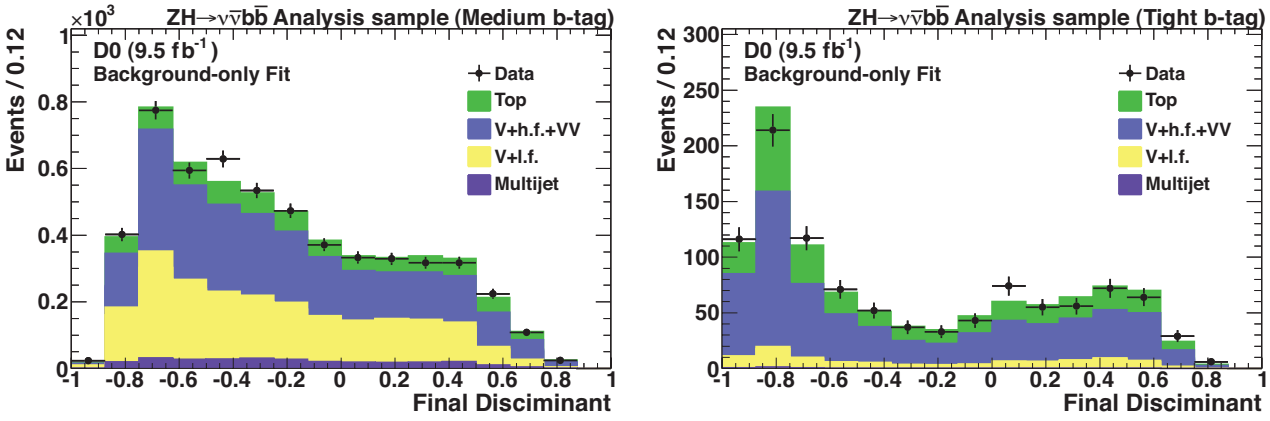

(a) (b)

FIG. 15: The SM DT output, for $m_H = 125$ GeV, following the multijet veto and after the fit to the data under the background-only hypothesis in the (a) medium and (b) tight b-tag channels. The data are shown as points and the background contributions as histograms: dibosons are labeled as "VV", "V+l.f." includes $(W/Z)+(u,d,s,g)$ jets, "V+h.f." includes $(W/Z)+(b,c)$ jets and "Top" includes pair and single top quark production.

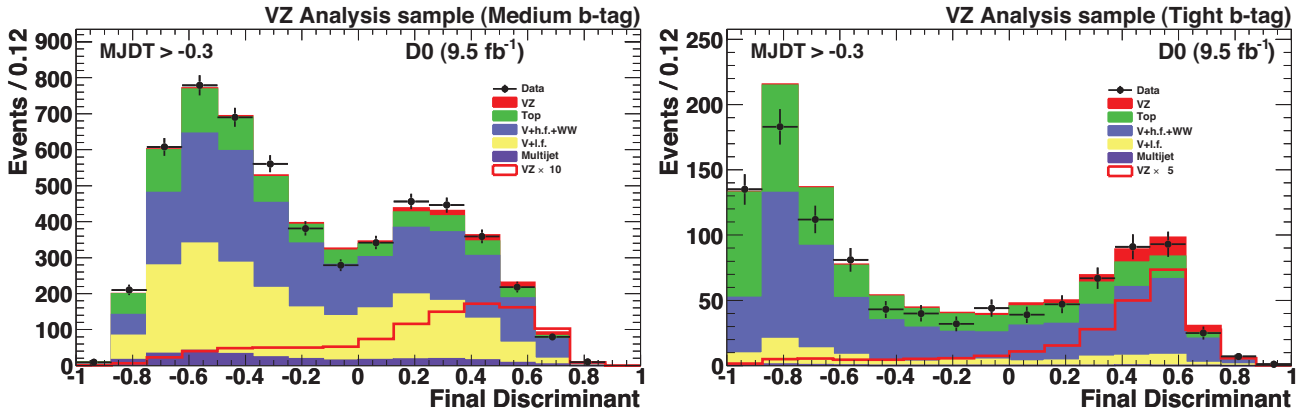

(a) (b)

FIG. 16: The SM DT output for the WZ and ZZ diboson search following the multijet veto for (a) medium and (b) tight tag prior to the fit to data. The data are shown as points and the background contributions as histograms; "V+l.f." includes $(W/Z)+(u,d,s,g)$ jets, "V+h.f." includes $(W/Z)+(b,c)$ jets and "Top" includes pair and single top quark production. The WZ and ZZ signal is denoted as VZ. The distributions for signal are scaled to the SM cross section (filled red histogram) and shown separately multiplied by a factor of 10 for medium b-tag and 5 for tight b-tag (solid red line) respectively.

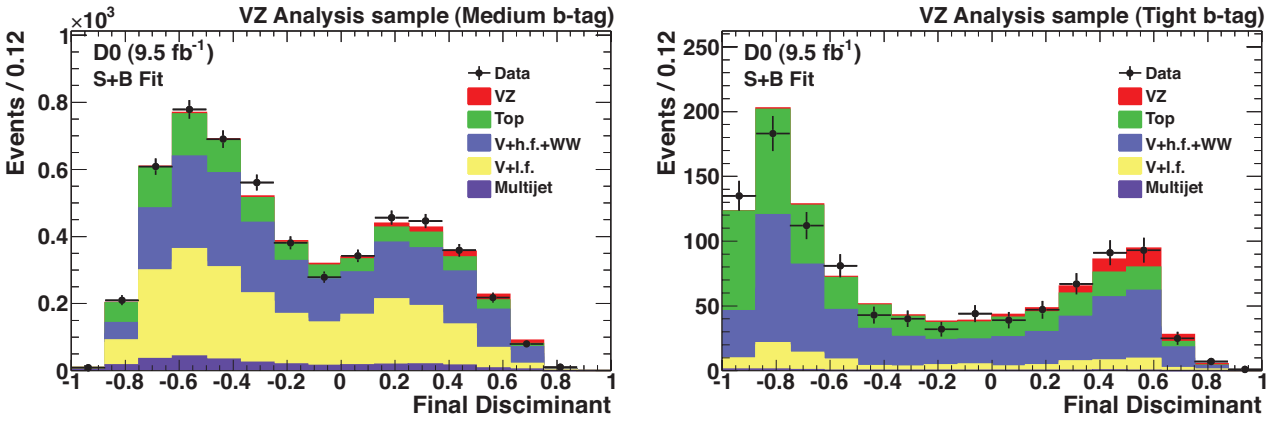

(a) (b)

FIG. 17: The SM DT output for the WZ and ZZ diboson search, following the multijet veto, and after the fit to the data under the signal+background hypothesis in the (a) medium and (b) tight tag channels. The data are shown as points and the background contributions as histograms; "V+l.f." includes $(W/Z)+(u,d,s,g)$ jets, "V+h.f." includes $(W/Z)+(b,c)$ jets and "Top" includes pair and single top quark production. The WZ and ZZ signal expectation (red histogram, and denoted VZ) is scaled to the SM cross section.

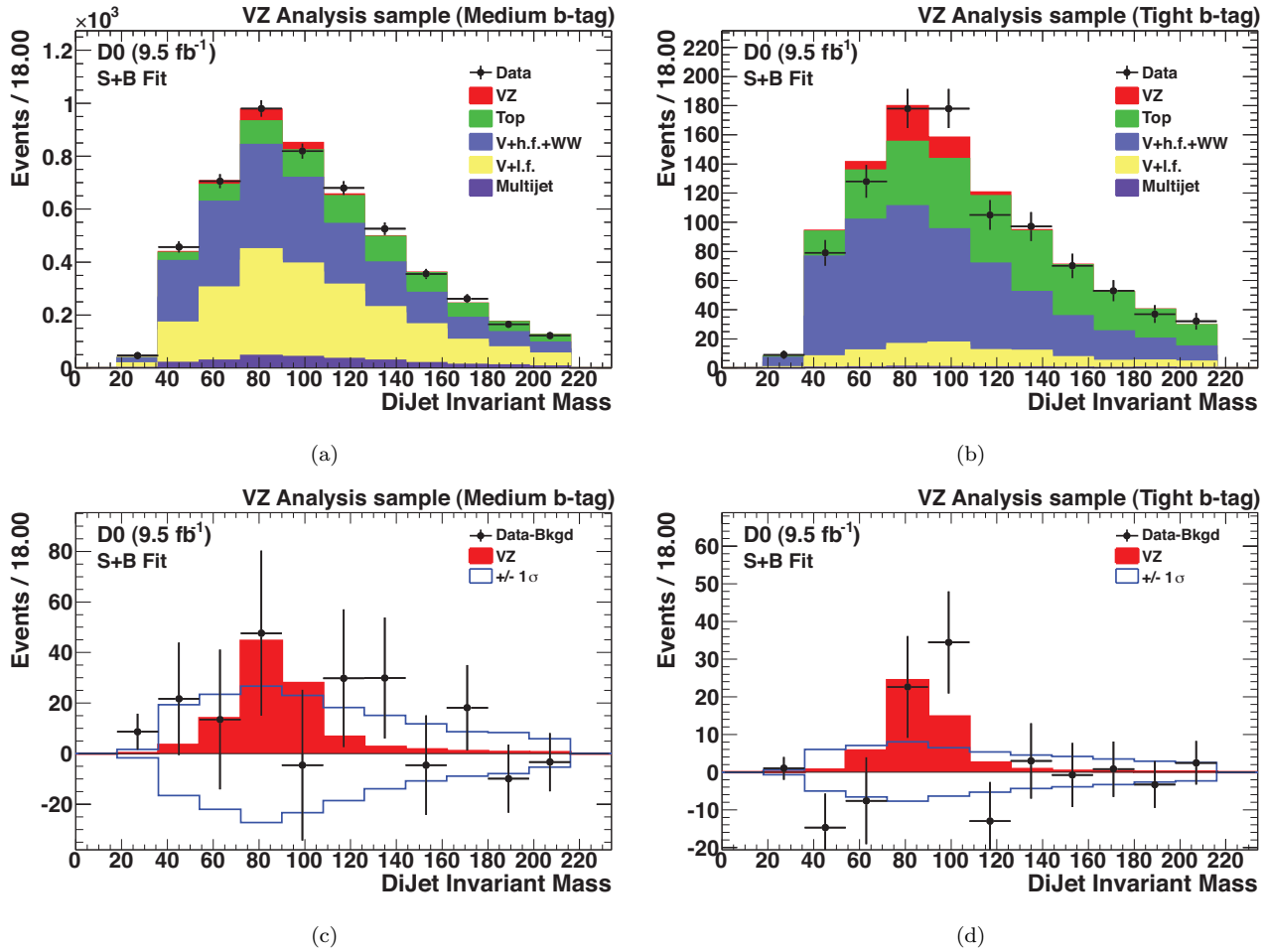

FIG. 18: The dijet invariant mass for the WZ and ZZ diboson search, following the multijet veto, and after the fit to the data under the signal+background hypothesis in the (a) medium and (b) tight tag channels. The data are shown as points and the background contributions as histograms; "V+l.f." includes $(W/Z)+(u,d,s,g)$ jets, "V+h.f." includes $(W/Z)+(b,c)$ jets and "Top" includes pair and single top quark production. The WZ and ZZ signal expectation (red histogram, and denoted VZ) and the data after subtracting the fitted background (points) are shown in the (c) medium and (d) tight tag channels. Also shown is the ± 1 standard deviation band on the total background after fitting. The signal is scaled to the SM cross section.